

Evidence for exceptional low temperature ductility in polycrystalline magnesium processed by severe plastic deformation

Roberto B. Figueiredo^{1,2}, Shima Sabbaghianrad², Adenike Giwa³,

Julia R. Greer³, Terence G. Langdon^{2,4}

¹Department of Materials Engineering and Civil Construction, Universidade Federal de Minas Gerais, Belo Horizonte 31270-901, MG, Brazil

²Departments of Aerospace and Mechanical Engineering & Materials Science, University of Southern California, Los Angeles, CA 90089-1453, U.S.A.

³Division of Engineering and Applied Sciences, California Institute of Technology, Pasadena, CA 91125, U.S.A.

⁴Materials Research Group, Faculty of Engineering and the Environment, University of Southampton, Southampton SO17 1BJ, U.K.

Abstract

An investigation was conducted to examine the mechanical behavior and microstructure evolution during deformation of ultrafine-grained pure magnesium at low temperatures within the temperature range of 296 - 373 K. Discs were processed by high-pressure torsion until saturation in grain refinement. Dynamic hardness testing revealed a gradual increase in strain rate sensitivity up to $m \approx 0.2$. High ductility was observed in the ultrafine-grained magnesium including an exceptional elongation of ~360% in tension at room temperature and stable deformation in micropillar compression. Grain coarsening and an increase in frequency of grain boundaries with misorientations in the range $15^\circ - 45^\circ$ occurred during deformation in tension. The experimental evidence, when combined with an analysis of the deformation behavior, suggests that grain boundary sliding plays a key role in low strain rate deformation of pure magnesium when the grain sizes are at and below $\sim 5 \mu\text{m}$.

Keywords: ductility; flow mechanisms; grain boundary sliding; high-pressure torsion; magnesium

*corresponding author: figueiredo@demc.ufmg.br

1. Introduction

The deformation behavior of magnesium has been studied for several decades but an increasing interest has developed recently because of the potential for using magnesium in a wide range of industrial applications. Nevertheless, the flow behavior of fine-grained magnesium remains an area of some controversy. For example, it is known that twinning plays a major role in the room temperature deformation of magnesium and it was shown that both twinning and dislocation slip are active to accommodate the high strain rate compressive deformation of pure magnesium having a grain size of $\sim 20\text{ }\mu\text{m}$ [1]. Twinning leads to a hard orientation of the crystalline structure and significant hardening is observed in the stress-strain curves [1]. Also, experiments show that the fraction of grains with twinning is independent of the grain area although grain areas smaller than $\sim 21\text{ }\mu\text{m}^2$, corresponding to grain diameters of $<5.25\text{ }\mu\text{m}$, were not considered [2]. However, a twinning to slip transition was reported in compression testing when reducing the grain size in an AZ31 magnesium alloy [3] and also in pure magnesium [4,5]. Moreover, there is some limited evidence for a grain boundary sliding contribution in plastic deformation at room temperature [6,7]. It was also reported that twinning is suppressed and the contribution of grain boundary sliding increases in magnesium with a grain size of $\sim 60\text{ nm}$, thereby producing an increased strain rate sensitivity and an inverse Hall-Petch relationship [8]. A Hall-Petch breakdown at low strain rates was demonstrated in magnesium but in samples with grain sizes of several microns [7].

It was shown recently that non-basal slip and twinning are severely hindered during tensile testing at 323 K when the grain size is reduced to $\sim 5\text{ }\mu\text{m}$ and this was interpreted in terms of an increase with grain refinement in the ratio of the critical resolved shear stress for non-basal to basal slip [9]. The accommodation of plastic deformation was attributed to a mechanism of strain propagation through boundaries with misorientations of $<35^\circ$. Thus, the

ductility of a sample with a grain size of 5 μm was lower than in samples with grain sizes of 19 and 36 μm and this was due directly to the limited strain accommodation by this mechanism [9]. Nevertheless, excellent ductilities were recorded in pure magnesium with even finer grain structures including an elongation of 230% in a sample with a grain size of 1.2 μm tested at room temperature at a low strain rate of 10^{-5} s^{-1} [7]. Good plasticity at room temperature was observed also in fine-grained magnesium tested at low strain rates [5]. In order to explain this different deformation behavior observed at low strain rates in fine-grained magnesium, a mechanism of strain accommodation was proposed based on basal slip and grain boundary rotation [5].

The present experiments were initiated in order to obtain a better understanding of the deformation mechanisms operating in pure magnesium at low temperatures when using samples with unusually fine grain structures. High-pressure torsion (HPT) [10] was used to produce contamination-free samples with ultrafine-grained structures and the material was tested using dynamic hardness, *in situ* micro-pillar compression and conventional tensile testing.

2. Experimental material and procedures

The material used in these experiments was commercial purity (CP) polycrystalline magnesium provided by RIMA (Bocaiúva-MG, Brazil). The material was received as a cast ingot with an average grain size of $\sim 300 \mu\text{m}$. Billets of 10 mm diameter were machined from the ingot and then discs with 1.0 mm thickness were cut from the billets using a low-speed diamond saw. Finally, the thicknesses of the discs were reduced to $\sim 0.85 \text{ mm}$ using grinding papers.

The discs were processed by high-pressure torsion using anvils that gave quasi-constrained conditions. In this processing condition, each anvil contains a shallow depression

having a depth of less than one-half of the disc thickness so that some limited material is extruded around the periphery of the disc during processing [11,12]. The samples were processed under a pressure of 6.0 GPa with a rotation rate of 1 rpm at room temperature. The maximum temperature rise in the sample was estimated as ~ 10 K [13] considering a reasonable flow stress of ~ 200 MPa. After processing by HPT, the average disc thickness was ~ 0.72 mm which corresponded to a reduction in thickness of $\sim 15\%$. Samples were processed to totals of 1/8, 1/2, 2 and 10 turns which correspond to effective strains [14,15] of approximately 1.4, 5.8, 23.1 and 115.5, respectively, at the mid-radius position of $r = 2.5$ mm where r is the disc radius.

After processing, all samples were prepared for electron backscatter diffraction (EBSD) characterization by grinding with abrasive paper #2500 and polishing with 9-, 6-, 3- and 1- μ m diamond suspensions and a colloidal silica suspension. Final polishing was conducted using a Vibromet facility with a blue colloidal silica suspension for 1 h. The microstructures of the processed discs were evaluated by EBSD using a JEOL JSM-7001F scanning electron microscope (SEM) operating at 7 kV and the data were collected and analyzed using TSL orientation imaging microscopy (OIM) and appropriate software with a step size of 0.1 μ m. All microstructures were observed at the mid-radius positions and Kikuchi patterns were obtained at a working distance of 15 mm with a sample tilt of 70° . The images were cleaned up using grain confidence index (CI) standardization, neighbor CI correlation and grain dilation procedures.

Dynamic hardness testing was performed using a Shimadzu DUH-211S hardness facility equipped with a Berkovich indenter. Tests were conducted using a maximum load of 300 mN, a loading rate of 70 mN s^{-1} and a dwell time of 500 s. The data for the indenter depth, h , and testing time, t , were converted to strain rate, $\dot{\epsilon}_{\text{eff}}$, using the relationship [16-18]

$$\dot{\epsilon}_{\text{eff}} = C \times (1/h) \left(dh/dt \right) \quad (1)$$

where C is a constant equal to 0.1 [18]. The hardness, H , was converted to flow stress, σ , using [18]

$$\sigma = H/\alpha \quad (2)$$

where α is a correlation factor equal to 3.3. The strain rate sensitivity was determined as the slope of the curve of flow stress, σ , plotted as a function of strain rate, $\dot{\epsilon}$.

Tensile specimens with gauge lengths of 1.0 mm and cross-sectional areas of $1.0 \times 0.72 \text{ mm}^2$ were extracted from the processed discs at the mid-radius positions using electro-discharge machining. These specimens were tested in tension at room temperature (296 K) using an Instron machine operating at a constant rate of cross-head displacement. The load and displacement data were converted to engineering stress and engineering strain and the influence of the elastic distortion of the testing apparatus was minimized by equating the elastic portion of the stress-strain curves to the theoretical elastic modulus of magnesium. Tests were performed with initial strain rates in the range of $10^{-5} - 10^{-1} \text{ s}^{-1}$. Some specimens were also annealed at 373 K for 24 h before testing in tension at 296, 323 and 373 K. The gauge length of a tensile sample was polished prior to testing at a strain rate of 10^{-5} s^{-1} , the test was interrupted at an elongation of 50% and the surface was analyzed by SEM. Further polishing was then conducted to prepare for EBSD. Finally, the gauge lengths of some samples were polished for EBSD analysis near the crack tips after pulling to failure.

Two micro-pillars were fabricated from the material processed through 10 turns of HPT using focused ion beam (FIB) machining [19-21] with the surfaces of these discs prepared using the same procedure as for EBSD characterization. These two pillars had diameters of ~ 1.77 and $\sim 1.73 \text{ }\mu\text{m}$ and lengths of ~ 6.16 and $\sim 5.19 \text{ }\mu\text{m}$, respectively. The

micro-pillar compression experiments were performed using a nanoindenter (Triboscope, Hysitron Inc.) equipped with a custom-made flat punch compression tip. The micro-compressions were conducted at a constant nominal displacement rate corresponding to a prescribed strain rate of 10^{-3} s^{-1} .

3. Experimental results

3.1 Microstructures after HPT

The microstructures of CP magnesium at different stages of processing by HPT are shown in the inverse pole figures in Fig. 1. Inspection shows that significant areas with fine grains are observed even in the sample processed through only 1/8 turn together with areas of coarser grains. Most of these coarse grains exhibit twinning. The area fraction of fine grains increases with increasing deformation and so that fine grains occupy most of the microstructure after 1/2 turn. This gradual refinement of a coarse-grained structure matches a model of grain refinement proposed for magnesium deformed at high temperatures [22,23] and shows that a similar mechanism also occurs at room temperature. After 1/2 turn of HPT, there are only a few coarser grains in the microstructure with sizes of $\sim 1 - 3 \text{ }\mu\text{m}$. Nevertheless, these coarser grains are also present even after 10 turns of HPT although their area fraction has decreased significantly. Thus, the microstructure is composed essentially of ultrafine grains after 10 turns of HPT which is consistent with earlier reports using TEM analysis [5,24].

3.2 Dynamic hardness testing

The evolution of flow stress as a function of the effective strain rate was determined by dynamic hardness testing at the mid-radius of the discs at different stages of HPT processing. Figure 2 shows the curves for samples processed by 1/8, 1/2, 2 and 10 turns of HPT. The flow stress of the material processed by only 1/8 turn varies slightly from ~ 115

MPa at the lowest strain rate to ~143 MPa at the highest strain rate. However, the slopes of the curves increase with increasing numbers of turns in HPT and this is associated with a decrease in the flow stress at the lower strain rates whereas there are only minor variations at the higher strain rates. Thus, the flow stresses at a strain rate of $\sim 2 \times 10^{-5} \text{ s}^{-1}$ are ~88 and ~67 MPa after processing through 1/2 and 2 turns of HPT, respectively, and these values increase to ~141 and ~133 MPa at $\sim 1 \times 10^{-3} \text{ s}^{-1}$, respectively. It is important to note also that these curves exhibit essentially no variation between 2 and 10 turns which suggests that the mechanical behavior of the material is not changed after 2 turns. A similar trend of increasing slope with decreasing grain size was observed in dynamic hardness testing in an earlier report using magnesium in the as-cast condition and processing by equal-channel angular pressing (ECAP) and HPT [5].

The slope of the curves of flow stress plotted against strain rate corresponds to the strain rate sensitivity, m . Thus, multiple tests were performed at different locations on the discs processed by 1/8, 1/2 and 2 turns of HPT and the average slopes of the curves were determined. Figure 3 shows the evolution of strain rate sensitivity as a function of the accumulated strain in HPT. It is observed that the value of the strain rate sensitivity increases from ~0.05 in the early stage of processing to ~0.20 after a strain of ~15 and thereafter remains essentially constant. An increase in strain rate sensitivity was also detected by nano-indentation in a magnesium ZK60 alloy processed by HPT although the maximum value was <0.05 and the effect saturated after only 1/2 turn [25]. Also, a stress exponent of ~4, corresponding to a strain rate sensitivity of ~0.25, was reported during the nanoindentation creep testing of pure magnesium with a grain size of 2 μm [26].

3.3 Tensile testing

Tensile tests were conducted at different strain rates in samples processed by 10 turns of HPT and Fig. 4 shows the appearance of the specimens and their final elongations after

pulling to failure at different strain rates. Thus, the specimen pulled at the fastest strain rate exhibits no significant deformation within the gauge length. However, samples pulled at strain rates at and below 10^{-2} s^{-1} exhibit significant reductions of the gauge areas which are associated with fairly high ductilities. The sample tested at the lowest strain rate of 10^{-5} s^{-1} exhibited an exceptional elongation of $\sim 360\%$ which is high for CP magnesium at room temperature. The various elongations observed in these samples are plotted as a function of strain rate in Fig. 5 together with the elongations observed in samples annealed for 24 h at 373 K and then tested at 296 or 373 K: in these plots, ΔL is the increase in length and L_0 is the initial gauge length. The as-processed material generally exhibits larger elongations compared to their annealed counterpart although a high elongation of $\sim 180\%$ was obtained after annealing at 296 K at the lowest strain rate. Testing at the higher temperature of 373 K led to an increase in ductility of the annealed material such that elongations of $\sim 100\%$ and higher were observed at strain rates at and below $\sim 10^{-2} \text{ s}^{-1}$.

The true stress vs. true strain curves of the material processed by HPT and tested at different strain rates without annealing are shown in Fig. 6(a). The flow stresses, defined as the stress at a true strain of 0.1, varies significantly from $\sim 250 \text{ MPa}$ at a strain rate of 10^{-1} s^{-1} to $\sim 50 \text{ MPa}$ at 10^{-5} s^{-1} . It is also apparent that the curves exhibit significant hardening and this effect is more obvious at the lower strain rates. The curves for the samples subjected to annealing at 373 K for 24 hours are also shown in Fig. 6(b) and (c) after testing at 296 or 373 K, respectively. It is observed that the flow stresses of the material tested at the lowest strain rates increase after annealing. The decrease in elongation and increase in flow stress observed after annealing are in agreement with recent results for magnesium processed by HPT and annealed at 523 K for 3 s [27]. The flow stress decreases when testing at 373 K but all curves show significant hardening.

Figure 7 shows the appearance of the surface of a specimen processed by HPT and tested in tension at 10^{-5} s^{-1} to an elongation of 50%. Slip lines were not readily observed in this specimen but the grain boundaries revealed sharp offsets which are consistent with the occurrence of significant grain boundary sliding during deformation.

3.4. Microstructural evolution during tensile testing

The microstructures within the gauge areas of tensile specimens pulled to an elongation of 50% and after failure at 360% at room temperature are shown in Fig. 8 together with the grain boundary misorientation angle distributions and inverse pole figures after testing at 10^{-5} s^{-1} . Thus, the grain size increases during testing and the mean linear intercept length increases from ~320 nm before testing to ~490 nm after 50% elongation and then to ~750 nm after failure at 360%. The grain boundary misorientation distribution shows a high frequency in the range $15^\circ\sim 45^\circ$ before testing, an increase in this frequency range and a decrease in frequency for misorientations larger than 70° at low strains (up to 50% elongation). High frequency of grain boundary misorientations $<45^\circ$ is predicted for a random distribution in magnesium with a basal fiber texture [28]. High intensities of misorientations in this range were reported in pure magnesium with high ductility subjected to compressive deformation up to a true strain of 1.0 at room temperature [29]. However, the increase in frequency of misorientations $<45^\circ$ during tensile deformation up to 50% elongation does not agree with a random rotation of grains since in this case a randomization of grain boundary misorientation distribution would be expected. This suggests rotation of grains towards a preferential orientation. It has been shown that basal slip can propagate through grain boundaries with misorientations $<35^\circ$ in pure magnesium with fine grain sizes [9]. Hence, the present results suggest grain boundaries with low misorientations are more stable during deformation in fine grained magnesium. Further tensile deformation (up to 360% elongation) promotes a slight increase in misorientations in the range of 30° to 70°

although the majority of the grain boundaries continues to exhibit misorientations $<35^\circ$. It is worth noting that the frequency of grain boundaries with misorientations $<45^\circ$ after 360% elongation is larger than the initial distribution which also supports the assumption of a higher stability of this misorientation range in fine-grained magnesium. It should be noted that the frequency of misorientations $>80^\circ$ decreases during tensile deformation up to 50% elongation which suggests twinning does not play a major role during deformation since the twinning in magnesium is expected to promote a rotation of $\sim 86^\circ$ of the lattice [30]. This is in agreement with the reduced activity of twinning in fine-grained magnesium reported elsewhere [9].

The inverse pole figures show a slight trend of decreasing the frequency of grains with the $\langle 2\bar{1}\bar{1}0 \rangle$ direction aligned with the tensile axis. They also show an increase in intensities of grains with c-axis perpendicular to the tensile direction and an increase in maximum intensity during tensile deformation. An increase in maximum intensity of texture was reported during high temperature tensile deformation of a magnesium alloy with reduced contribution of grain boundary sliding while a decrease in intensity was reported in conditions with a high contribution of grain boundary sliding [31].

The microstructure of the material subjected to annealing after HPT processing is shown in Fig. 9 before and after testing at 10^{-5} s^{-1} at 373 K. Grain growth is also observed during tensile testing in this condition with the mean linear intercept length increasing from $\sim 0.95 \text{ }\mu\text{m}$ in the annealed condition to $\sim 2.29 \text{ }\mu\text{m}$ after 260% elongation. The grain boundary misorientation distribution also shows a peak at 30° before testing and this distribution is retained during tensile deformation up to 260% elongation. A peak at 30° in grain boundary misorientation distribution was also observed in a rolled magnesium alloy AZ31 and conserved during tensile testing at 648 K up to $\sim 320\%$ elongation under conditions in which grain boundary sliding played a major role [32]. The persistence of the basal fiber texture

during high temperature deformation was attributed to the concurrent operation of crystallographic slip [32]. This is in agreement with the present results despite the difference in testing temperature.

3.5 Micropillar compression testing

The true stress vs. strain data obtained during compression of a micro-pillar with diameter of $\sim 1.77 \mu\text{m}$ is shown in Fig. 10, together with an SEM image of the same micropillar after $\sim 15\%$ compressive strain. This material was tested after 10 turns of HPT processing and the stress-strain data show a minor post-yield softening up to a strain of $\sim 10\%$ and then subsequent hardening. The flow stress remained within a narrow range of $\sim 194\sim 222$ MPa and no strain bursts or avalanches were detected throughout the compression. This flow stress is higher than the value typically observed during compression of single crystal Mg micropillars oriented for basal slip (~ 100 MPa [33] and ~ 60 MPa [34]) but it is lower than the flow stress in samples of similar diameter with basal planes oriented perpendicular to the compression direction (~ 300 MPa [33]). The available data shows that the flow stress of single crystal Mg micropillars oriented for twinning is low, of the order of ~ 100 MPa in the early stages of deformation, and subsequently rises to >600 MPa at a strain of $\sim 15\%$ [34]. In practice, the polycrystalline micropillar attains a rough surface after compression, with lateral bulges having sizes similar to the grain size of the material. This differs significantly from the appearance of single crystal micro-pillars where failure occurs by severe slip along the basal planes [33,34].

4. Discussion

The present results demonstrate the occurrence of a clear change in deformation behavior for magnesium where grain refinement is introduced through high-pressure torsion. The change in the strain rate sensitivity determined by dynamic hardness testing agrees well

with the grain refinement observed by EBSD. The coarse-grained initial material exhibits a low strain rate sensitivity and this parameter increases as the fraction of ultrafine grains increases in the microstructure, ultimately reaching a saturation after accumulated strains of ~ 15 . This increase in strain rate sensitivity is associated with a significant increase in the ductility of magnesium.

4.1 An examination of the enhanced ductility

Commercial purity magnesium usually exhibits poor ductility at room temperature. For example, as-cast magnesium exhibits less than 10% elongation in tension when testing at a strain rate of $3.3 \times 10^{-5} \text{ s}^{-1}$ [35] and rolled magnesium exhibits less than 5% elongation at a strain rate of $1.7 \times 10^{-3} \text{ s}^{-1}$ [36]. Nevertheless, the present results show elongations larger than 100% in HPT-processed magnesium at strain rates at and below 10^{-3} s^{-1} including an exceptional elongation of $\sim 360\%$ at 10^{-5} s^{-1} . This result is in agreement with the improved ductility with grain refinement reported in early experiments on magnesium [37] including an elongation of 230% in a sample with a grain size of $\sim 1.2 \text{ }\mu\text{m}$ [7]. Higher ductility was also reported in an HPT-processed magnesium tested at 10^{-3} s^{-1} compared to its annealed counterpart [27].

Some enhanced ductility was reported in fine-grained magnesium deformed in compression at low strain rates. For example, a recent report showed that magnesium processed by ECAP, with a grain size of $\sim 2.8 \text{ }\mu\text{m}$, deformed without failure to a strain of $>35\%$ in compression at a strain-rate of 10^{-6} s^{-1} while its coarser-grained counterpart failed at a strain of $<20\%$ [5]. Improved plasticity was also reported during compression of magnesium processed by ECAP with a grain size of $0.8 \text{ }\mu\text{m}$ [38].

The present results provide significant insight into the plasticity associated with micro-pillar compression. A compressive strain of $\sim 15\%$ was attained without any bursts in

the stress-strain data and without any evidence of shear failure in the pillar. The orientations of the basal planes with respect to the loading direction are known to play a key role in micro-pillar compression of Mg single crystals where failure usually occurs via basal slip [39]. Shear instability due to basal slip was reported during micro-pillar compression along the (0001) axis [39]. Twinning was also reported to contribute to plastic deformation of micro-pillar compression of Mg single crystals, characterized by a pronounced hardening in the stress-strain data [34]. Failure caused by basal slip was reported in a magnesium AZ31 alloy oriented for basal slip during nano-pillar compression and also in samples oriented for pyramidal slip with a few degrees of misalignment [40].

High plasticity during micro-pillar compression was reported in a Mg-10 wt.% Al nanocrystalline alloy and this effect was attributed to the introduction of nanotwins and a bimodal grain size distribution [41]. High strength and ductility was also reported in Mg-2% Zn with 14 vol.% SiC nanoparticles [42]. In the latter example, the dense distribution of nanoparticles served to block dislocation slip on the basal planes and thereby suppressed the characteristic multiple slip bands observed in samples without nanoparticles. By contrast, the samples in the present investigation failed to exhibit either a bimodal grain size distribution or a dense distribution of nanoparticles. Therefore, it is concluded that the improved ductility and absence of multiple slip traces in the compressed micro-pillars is due to the activation of a different deformation mechanism. Furthermore, the micro-pillar surfaces showed evidence of bulges which might suggest an inhomogeneous strain distribution and a contribution to the deformation from grain boundary sliding. A similar effect was observed in an Al-30% Zn alloy in which coarse-grained samples exhibited avalanches in the load-displacement curves during micro-pillar compression while nanocrystalline samples exhibited stable deformation [43]. Thus, the compressed micro-pillars showed evidence of extreme slip in the coarse-grained samples while the nanocrystalline samples exhibited no slip traces but significant

grain boundary sliding [43]. These earlier results are consistent with the present investigation where the appearance of the surface of a sample of magnesium processed by HPT and tested in tension, as shown in Fig. 7, also supports grain boundary sliding as a dominant deformation mechanism.

4.2 The deformation process

The flow stresses obtained in the present tensile tests, defined as the true stress at a true strain of 0.1, are plotted as a function of strain rate in Fig. 11 together with data from recent reports for the room temperature testing of fine-grained pure magnesium [5,7]. The grain size, d , in the present experiments, and in the early report of magnesium processed by ECAP [5], was determined as $d = 1.74 \times L$, where L is the mean linear intercept length [44]. Higher slopes are observed at low strain rates and a transition towards reduced slopes takes place with increasing strain rate. However, this transition occurs at lower strain rates with increasing grain size. For example, the transition to a higher slope occurs at $\sim 10^{-2} \text{ s}^{-1}$ for a grain size of $\sim 0.56 \text{ }\mu\text{m}$ and at $\sim 10^{-6} \text{ s}^{-1}$ for a grain size of $\sim 5.57 \text{ }\mu\text{m}$.

The high slope in the stress vs strain rate curves suggests the occurrence of a creep mechanism operating at room temperature in pure magnesium where the grain size plays an important role. The creep rate, $\dot{\epsilon}$, is usually described by the following equation:

$$\dot{\epsilon} = \frac{AGb}{kT} D_0 \exp\left(\frac{-Q}{RT}\right) \left(\frac{b}{d}\right)^p \left(\frac{\sigma}{G}\right)^n \quad (3)$$

where A is a constant, G is the shear modulus, b is the Burgers vector modulus, k is the Boltzmann constant, T is the absolute temperature, D_0 is a frequency factor, Q is the activation energy for diffusion, R is the gas constant, p is the inverse grain size exponent and n is the stress exponent. In order to determine the creep equation for the rate-controlling

mechanism taking place in fine-grained pure magnesium at low strain rates, it is necessary to determine the values of Q , p and n .

The grain size exponent may be determined by plotting the strain rate, at a constant testing temperature and stress, as a function of the inverse of the grain size. This plot is shown in Fig. 12 for a stress of 100 MPa and with the strain rate determined as the intercept between the trend curves shown in Fig. 11 and the flow stress of 100 MPa. It is clear from Fig. 12 that the slope is well-defined at $p \approx 2.5$.

The activation energy for diffusion may be determined by plotting the flow stress, σ , as a function of the inverse of the testing temperature, T , for samples with similar grain size and tested at similar strain rate using the relationship [45]

$$Q = nR \left[\frac{\partial \ln \sigma}{\partial \left(\frac{1}{T} \right)} \right]_{d, \dot{\epsilon}(\text{const})} \quad (4)$$

Tensile tests were carried out at a strain rate of 10^{-5} s^{-1} at 296, 323 and 373 K for samples annealed at 373 K for 24 h where this annealing treatment was selected to prevent grain growth before tensile testing at the heat treatment temperature. Figure 13 shows this plot with a slope of $Q \approx 75 \text{ kJ mol}^{-1}$ for the present data where this is lower than the activation energy for grain boundary diffusion of $\sim 92 \text{ kJ mol}^{-1}$ and significantly lower than the value of $\sim 135 \text{ kJ mol}^{-1}$ for self-diffusion in magnesium [46]. However, the measured activation energy is in agreement with the value of $\sim 75 \text{ kJ mol}^{-1}$ obtained for compression testing of magnesium processed by ECAP [5] and also with a value of $\sim 75 \text{ kJ mol}^{-1}$ reported for tensile testing of magnesium with a grain size of $\sim 1.2 \text{ } \mu\text{m}$ [7]. These observations suggest that an enhanced diffusion mechanism takes place in fine-grained magnesium which explains the occurrence of creep at room temperature.

The experimental data for the strain rate normalized by the effect of grain size and temperature, taking $p \approx 2.5$ and $Q \approx 75 \text{ kJ mol}^{-1}$, is plotted in Fig. 14 as a function of the flow stress normalized by the shear modulus where $G = (19,200 - 8.6 T) \text{ MPa}$ and T is the temperature in degrees Kelvin [47]. Data are shown from dynamic hardness and tensile testing of the material processed through 10 turns of HPT and then subjected to tensile testing at 296, 323 and 373 K, for samples subjected to annealing and results from published reports documenting compression testing at different temperatures and tensile testing at low strain rates for magnesium processed by ECAP [5] and tensile testing of magnesium at different temperatures for samples with different grain sizes processed by extrusion [7]. These data show excellent agreement especially when it is noted that the range of grain size is approximately one order of magnitude, the results incorporate different testing methods and the temperature range covers from room temperature to 423 K. It is apparent also from Fig. 14 that there is a slope of $n \approx 5$ which gives a strain rate sensitivity of ~ 0.2 . This latter value is consistent with the value obtained from dynamic hardness testing and tensile testing of the material processed by HPT as shown in Fig. 11.

4.3 Analysis of creep mechanisms operating in magnesium

The creep rates observed in the present experiments are larger than expected for coarse-grained pure magnesium. Earlier reports analyzed the creep behavior of pure magnesium in the temperature ranges of 423 – 523 K [48] and 473 – 820 K [49]. A strain rate of $\sim 3 \times 10^{-7} \text{ s}^{-1}$ was reported for an applied stress of 35 MPa at a temperature of 423 K in a sample with a grain size of $\sim 100 \text{ }\mu\text{m}$ [48] and a strain rate of $\sim 2 \times 10^{-6} \text{ s}^{-1}$ was reported for a stress of $\sim 32 \text{ MPa}$ at 473 K with a grain size of $\sim 80 \text{ }\mu\text{m}$ [49]. A lower flow stress of $\sim 24 \text{ MPa}$ was observed in the present experiments at the lower temperature of 373 K for a faster strain rate of 10^{-5} s^{-1} . This demonstrates that the fine grain structure in the present experiments plays a critical role in determining the creep deformation mechanism.

Grain boundary sliding is a possible creep mechanism where this flow process is well-defined by a theoretical model [50] and supported by comprehensive analyses that show the mechanism satisfactorily accounts for the occurrence of superplasticity at high temperatures in ultrafine-grained metals processed by ECAP or HPT including in magnesium alloys [51,52]. The grain size exponent for this mechanism is $p = 2$ which is consistent with the present results in Fig. 12 but the stress exponent is $n \approx 2$ which is smaller than the value of $n \approx 5$ recorded in the present investigation in Fig. 14. Furthermore, sliding is controlled by grain boundary diffusion which requires an activation energy of $\sim 92 \text{ kJ mol}^{-1}$ in magnesium and this is larger than the value of $Q \approx 75 \text{ kJ mol}^{-1}$ observed in these experiments. This means the measured activation energy leads to an increase by a factor of $\sim 1000\times$ in the rate for grain boundary diffusion at a temperature of 296 K.

Despite these apparent deviations from the theoretical model, the present trend is consistent with extensive diffusion data, mainly for polycrystalline nickel, showing enhanced atomic diffusion in nanostructured materials due to the high population of lattice defects introduced when processing by severe plastic deformation [53]. The results suggest, therefore, that enhanced diffusion can lead to a significant contribution from grain boundary sliding in fine-grained magnesium at room temperature and this is supported both by direct evidence for the occurrence of sliding on the surface of a tensile specimen pulled to an elongation of 50% in Fig. 7 and by the development of small bulges on the surface of a micro-pillar after compression to 15%.

A recent report showed that the contribution of twinning and non-basal slip decreases with decreasing grain size in magnesium and there is slip propagation in basal planes through grain boundaries with misorientations $< 35^\circ$ [9]. Therefore, most plastic deformation in fine-grained magnesium takes place by basal slip along bands of grains with low misorientations but this mechanism can only accommodate a limited amount of deformation [9]. The present

results show that further refinement of the grain structure activates grain boundary sliding and this mechanism can accommodate part of the plastic strain by grain displacement. Furthermore, the present results also show an increase in texture intensities and an increase in fraction of grain boundaries with misorientations $<35^\circ$ which suggests grain rotation towards orientations that favor slip transfer between grains. A model for deformation accommodation by grain rotation and slip transfer was proposed recently [5] and the present results provide further supporting evidence for this model.

5. Summary and conclusions

1. Pure magnesium was processed by HPT and subjected to mechanical testing by dynamic hardness, tension and micro-pillar compression. The results show that grain refinement by severe plastic deformation leads to an increasing strain rate sensitivity up to a saturation at $m \approx 0.2$ at strains above ~ 15 . Elongations larger than 100% were observed at strain rates up to 10^{-3} s^{-1} including an exceptional elongation of $\sim 360\%$ at 10^{-5} s^{-1} at room temperature.

2. The improved ductility in the temperature range 296 K \sim 373 K is attributed to an enhanced contribution from grain boundary sliding to the overall deformation mechanism where this is supported by the increase in strain rate sensitivity, by grain boundary offsets observed on the surfaces of tensile specimens and by bulges on the surfaces of compressed micro-pillars.

3. Grain boundary sliding promotes grain rotation during deformation, which increases the fraction of grain boundaries with misorientations in the range of $15^\circ \sim 45^\circ$ and facilitates slip propagation between neighboring grains.

4. Within the low strain rate regime, the stress exponent was determined as $n \approx 5.0$, the exponent of the inverse grain size was $p \approx 2.5$ and the activation energy was $Q \approx 75 \text{ kJ mol}^{-1}$. The enhanced diffusion in this regime is due to the high population of lattice defects introduced by severe plastic deformation.

Acknowledgements

This work was supported in part by CNPq, FAPEMIG and CAPES of Brazil and in part by the National Science Foundation of the United States under Grant No. DMR-1160966.

References:

- [1] N. Dixit, K.Y. Xie, K.J. Hemker, K.T. Ramesh, Microstructural evolution of pure magnesium under high strain rate loading. *Acta Mater.* 87 (2015) 56-67.
- [2] I.J. Beyerlein, L. Capolungo, P.E. Marshall, R.J. McCabe, C.N. Tomé, Statistical analyses of deformation twinning in magnesium. *Phil. Mag.* 90 (2010) 2161-2190.
- [3] M.R. Barnett, Z. Keshavartz, A.G. Beer, D. Atwell, Influence of grain size on the compressive deformation of wrought Mg-3Al-1Zn. *Acta Mater* 52 (2004) 5093-5103.
- [4] C.M. Cepeda-Jiménez, J.M. Molina-Aldareguia, M.T. Perez-Prado, Origins of the twinning to slip transition with grain size refinement, with decreasing strain rate and with increasing temperature in magnesium. *Acta Mater.* 88 (2015) 232-244.
- [5] R.B. Figueiredo, F.S.J. Poggiali, C.L.P. Silva, P.R. Cetlin, T.G. Langdon, The influence of grain size and strain rate on the mechanical behavior of pure magnesium. *J. Mater. Sci.* 51 (2016) 3013-3024.
- [6] J. Koike, Enhanced deformation mechanisms by anisotropic plasticity in polycrystalline Mg alloys at room temperature. *Metall. Mater. Trans. A* 36 (2005) 1689-1696.
- [7] H. Somekawa, T. Mukai, Hall-Petch breakdown in fine-grained pure magnesium at low strain rates. *Metall. Mater. Trans. A* 46 (2015) 894.
- [8] H.J. Choi, Y. Kim, J.H. Shin, D.H. Bae, Deformation behavior of magnesium in the grain size spectrum from nano- to micrometer. *Mater. Sci. Eng. A* 527 (2010) 1565-1570.
- [9] C.M. Cepeda-Jiménez, J.M. Molina-Aldareguia, M.T. Perez-Prado, Effect of grain size on slip activity in pure magnesium polycrystals. *Acta Mater.* 84 (2015) 443-456.

- [10] A.P. Zhilyaev, T.G. Langdon, Using high-pressure torsion for metal processing: Fundamentals and applications. *Prog. Mater. Sci.* 53 (2008) 893-979.
- [11] R.B. Figueiredo, P.H.R. Pereira, M.T.P. Aguilar, P.R. Cetlin, T.G. Langdon, Using finite element modeling to examine the temperature distribution in quasi-constrained high-pressure torsion. *Acta Mater.* 60 (2012) 3190-3198.
- [12] P.H.R. Pereira, R.B. Figueiredo, P.R. Cetlin, T.G. Langdon, Using finite element modeling to examine the flow process and temperature evolution in HPT under different constraining conditions, *IOP Conf. Ser.: Mater. Sci. Eng.* 63 (2014) 012041 (10pp)
- [13] P.H.R. Pereira, R.B. Figueiredo, Y. Huang, P.R. Cetlin, T.G. Langdon, Modeling the temperature rise in high-pressure torsion, *Mater. Sci. Eng. A* 593 (2014) 185-188.
- [14] R.Z. Valiev, Yu. V. Ivanisenko, E.F. Rauch, B. Baudelet, Structure and deformation behaviour of armco iron subjected to severe plastic deformation, *Acta Mater.* 44 (1996) 4705-4712.
- [15] J.J. Jonas, C. Ghosh, L.S. Tóth, The equivalent strain in high pressure torsion, *Mater. Sci. Eng. A* 607 (2014) 530-535.
- [16] M.J. Mayo, W.D. Nix, A micro-indentation study of superplasticity in Pb, Sn, and Sn-38 wt% Pb, *Acta Metall.* 36 (1988) 2183-2192.
- [17] H. Somekawa, T. Mukai, Nanoindentation creep behavior of grain boundary in pure magnesium, *Phil. Mag. Lett.* 90 (2010) 883-890.
- [18] H. Somekawa, T. Mukai, Effect of grain boundary structures on grain boundary sliding in magnesium, *Mater. Lett.* 76 (2012) 32-35.

- [19] M.D. Uchic, D.M. Dimiduk, J.F. Florando, W.D. Nix, Sample dimensions influence strength and crystal plasticity, *Science* 305 (2004) 986-989.
- [20] J.R. Greer, W.C. Oliver, W.D. Nix, Size dependence of mechanical properties of gold at the micron scale in the absence of strain gradients, *Acta Mater.* 53 (2005) 1821.
- [21] J.R. Greer, W.D. Nix, Nanoscale gold pillars strengthened through dislocation starvation, *Phys. Rev. B* 73 (2006) 245410 (6pp).
- [22] R.B. Figueiredo, T.G. Langdon, Principles of grain refinement in magnesium alloys processed by equal-channel angular pressing. *J. Mater. Sci.* 44 (2009) 4758-4762.
- [23] R.B. Figueiredo, T.G. Langdon, Grain refinement and mechanical behavior of a magnesium alloy processed by ECAP. *J. Mater. Sci.* 45 (2010) 4827-4836.
- [24] K. Edalati, A. Yamamoto, Z. Horita, T. Ishihara, High-pressure torsion of pure magnesium: evolution of mechanical properties, microstructures and hydrogen storage capacity with equivalent strain. *Scr. Mater.* 64 (2011) 880-883.
- [25] I.-C. Choi, D.-H. Lee, B. Ahn, K. Durst, M. Kawasaki, T.G. Langdon, J. Jang, Enhancement of strain-rate sensitivity and shear yield strength of a magnesium alloy processed by high-pressure torsion. *Scr. Mater.* 94 (2015) 44-47.
- [26] C.L. Wang, T. Mukai, T.G. Nieh, Room temperature creep of fine-grained pure Mg: a direct comparison between nanoindentation and uniaxial tension. *J. Mater. Res.* 24 (2009) 1615-1618.
- [27] M. Joshi, Y. Fukuta, S. Gao, N. Park, D. Terada, N. Tsuji, Fabrication of fine recrystallized grains and their mechanical property in HPT processed pure magnesium. *IOP Conf. Ser.: Mater. Sci. Eng.* 63 (2014) 012074 (7pp)

- [28] J.A. del Valle, M.T. Pérez-Prado, O.A. Ruano, The distribution of disorientation angles in a rolled AZ31 Mg alloy. *Rev. Metal. Madrid* 38 (2002) 353-357.
- [29] K.D. Molodov, T. Al-Samman, D.A. Molodov, G. Gottstein, Mechanisms of exceptional ductility of magnesium single crystal during deformation at room temperature: Multiple twinning and dynamic recrystallization. *Acta Mater.* 76 (2014) 314-330.
- [30] P.G. Partridge, The crystallography and deformation modes of hexagonal close-packed metals. *Metall. Rev.* 12 (1967) 169-194
- [31] R. Panicker, A.H. Chokshi, R.K. Mishra, R. Verma, P.E. Krajewski, Microstructural evolution and grain boundary sliding in a superplastic magnesium AZ31 alloy. *Acta Mater.* 57 (2009) 3683-3693.
- [32] J.A. Del Valle, M.T. Pérez-Prado, O.A. Ruano, Deformation mechanisms responsible for the high ductility in a Mg AZ31 alloy analyzed by electron backscattered diffraction. *Metall. Mater. Trans. A* 36 (2005) 1427-1438.
- [33] C.M. Byer, K.T. Ramesh, Effects of the initial dislocation density on size effects in single-crystal magnesium. *Acta Mater.* 61 (2013) 3808-3818.
- [34] K.E. Prasad, K. Rajesh, U. Ramamurty, Micropillar and macropillar compression responses of magnesium single crystals oriented for single slip or extension twinning. *Acta Mater.* 65 (2014) 316-325.
- [35] K. Máthis, K. Nyilas, A. Axt, I. Dragomir-Cernatescu, T. Ungár, P. Lukáč, The evolution of non-basal dislocations as a function of deformation temperature in pure magnesium determined by X-ray diffraction. *Acta Mater.* 52 (2004) 2889-2894.

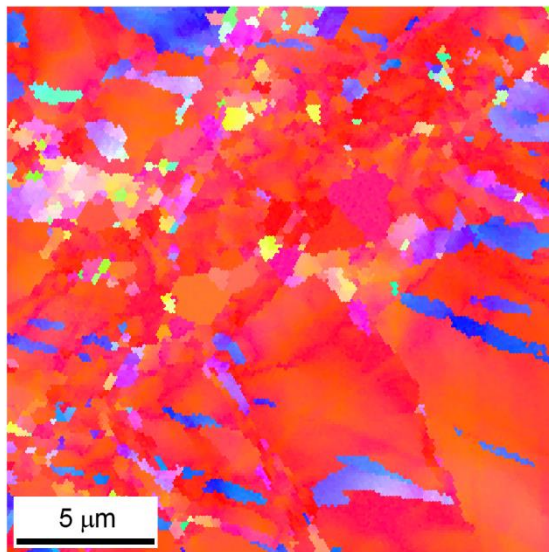
- [36] S. Sandlobes, S. Zaefferer, I. Schestakow, S. Yi, R. Gonzalez-Martinez, On the role of non-basal deformation mechanisms for the ductility of Mg and Mg-Y alloys. *Acta Mater.* 59 (2001) 429-439.
- [37] J.A. Chapman, D.V. Wilson, The room-temperature ductility of fine-grain Magnesium. *J. Inst. Metals* 91 (1962-63) 39-40.
- [38] J. Li, W. Xu, X. Wu, H. Ding, K. Xia, Effects of grain size on compressive behaviour in ultrafine grained pure Mg processed by equal channel angular pressing at room temperature. *Mater. Sci. Eng. A* 528 (2011) 5993-5998.
- [39] E. Lilleodden, Microcompression study of Mg (0001) single crystal. *Scr. Mater.* 62 (2010) 532-535.
- [40] Z.H. Aitken, H. Fan, J.A. El-Awady, J.R. Greer, The effect of size, orientation and alloying on the deformation of AZ31 nanopillars. *J. Mech. Phys. Solids* 76 (2015) 208-223.
- [41] M. Pozuelo, Y.W. Chang, J.-M. Yang, *In-situ* microcompression study of nanostructured Mg alloy micropillars. *Mater. Lett.* 108 (2013) 320-323.
- [42] L.-Y. Chen, J.-Q. Xu, H. Choi, M. Pozuelo, X. Ma, S. Bhowmick, J.-M. Yang, S. Mathaudhu, X.-C. Li, Processing and properties of magnesium containing a dense uniform dispersion of nanoparticles. *Nature* 528 (2015) 539-543.
- [43] N.Q. Chinh, T. Györi, R.Z. Valiev, P. Szommer, G. Varga, K. Havancsák, T.G. Langdon, Observation of unique plastic behavior in micro-pillars of an ultrafine-grained alloy. *MRS Communications* 2 (2012) 75-78.
- [44] F.A. Mohamed, T.G. Langdon, Creep at low stress levels in the superplastic Zn-22% Al eutectoid. *Acta Metall.* 23 (1975) 117-124.

- [45] F.A. Mohamed, T.G. Langdon, The determination of the activation energy for superplastic flow. *Phys. Status Solidi (a)* 33 (1976) 375-381.
- [46] H.J. Frost, M.F. Ashby, Deformation-mechanism maps: the plasticity and creep of metals and ceramics. Pergamon-Press, Oxford (1982).
- [47] S.S. Vagarali, T.G. Langdon, Deformation mechanisms in h.c.p. metals at elevated temperatures-II. Creep behavior of a Mg-0.8% Al solid solution alloy. *Acta Metall.* 30 (1982) 1157-1170.
- [48] L. Shi, D.O. Northwood, Strain-hardening and recovery during the creep of pure polycrystalline magnesium. *Acta Metall. Mater.* 42 (1994) 871-877.
- [49] S.S. Vagarali, T.G. Langdon, Deformation mechanisms in h.c.p. metals at elevated temperatures-I. Creep behavior of magnesium. *Acta Metall.* 29 (1981) 1969-1982.
- [50] T.G. Langdon, A unified approach to grain-boundary sliding in creep and superplasticity. *Acta Metall. Mater.* 42 (1994) 2437-2443.
- [51] M. Kawasaki, T.G. Langdon, Review: achieving superplasticity in metals processed by high-pressure torsion. *J. Mater. Sci.* 49 (2014) 6487-6496.
- [52] M. Kawasaki, T.G. Langdon, Review: achieving superplastic properties in ultrafine-grained metals at high temperatures. *J. Mater. Sci.* 51 (2016) 19-32.
- [53] S.V. Divinski, G. Reglitz, H. Rösner, Y. Estrin, G. Wilde, Ultra-fast diffusion channels in pure Ni severely deformed by equal-channel angular pressing. *Acta Mater.* 59 (2011) 1974-1985.

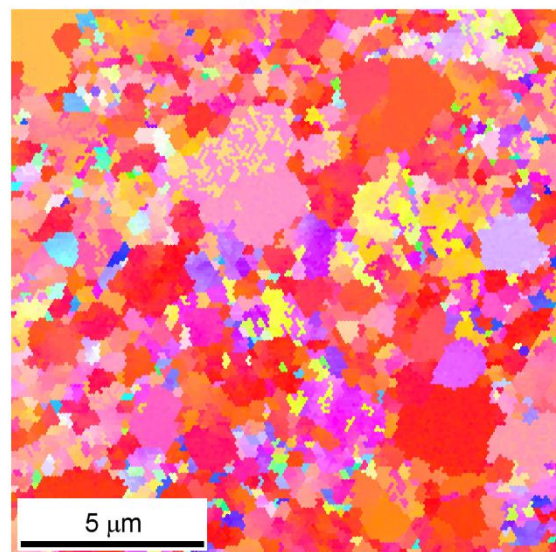
Figure captions

- Figure 1 – Inverse pole figure maps of the microstructures at the mid-radius positions of samples processed by 1/8, 1/2 and 10 turns of HPT.
- Figure 2 – Flow stress plotted as a function of the effective strain rate in dynamic hardness tests.
- Figure 3 – Evolution of the strain rate sensitivity, m , as a function of the accumulated strain during HPT.
- Figure 4 – Appearance of the tensile specimens of samples processed by 10 turns of HPT and pulled to failure at different strain rates.
- Figure 5 – Maximum elongations observed in samples of magnesium processed by HPT and tested in tension before and after annealing plotted as a function of the strain rate.
- Figure 6 – True stress vs true strain curves for tensile testing of samples (a) processed by HPT and after annealing and testing at (b) room temperature and (c) 373 K.
- Figure 7 – Surface of tensile specimen processed by HPT and tested in tension at 10^{-5} s^{-1} to an elongation of 50%.
- Figure 8 – Microstructures, grain boundary misorientation angle distributions and inverse pole figures in the gauge lengths of tensile specimens tested at room temperature at 10^{-5} s^{-1} to elongations of 50% and 360%.
- Figure 9 – Microstructures and grain boundary misorientation angle distributions in the gauge lengths before and after testing for tensile specimens processed by HPT and subjected to annealing.
- Figure 10 – Stress-strain curve determined by micropillar compression of a material processed by 10 turns of HPT (upper) and the appearance of the micropillar after ~15% strain (lower).
- Figure 11 – Flow stress observed in tensile testing of fine-grained pure magnesium plotted as a function of the strain rate using the present results and published data [5,7].
- Figure 12 – Strain rate at a stress of 100 MPa plotted as a function of the inverse of the grain size using the present results and published data [5,7].
- Figure 13 – Flow stress in the material annealed after HPT processing for tests at a strain rate of 10^{-5} s^{-1} plotted as a function of the inverse of the testing temperature.
- Figure 14 – Strain rate normalized by temperature and grain size plotted as a function of the flow stress normalized by the shear modulus for pure magnesium using the present results and reported data [5,7].

CP-Mg
HPT: 6.0 GPa (296 K) 1 rpm
N = 1/8



N = 1/2



N = 10

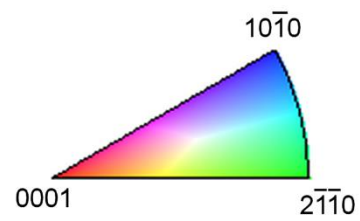
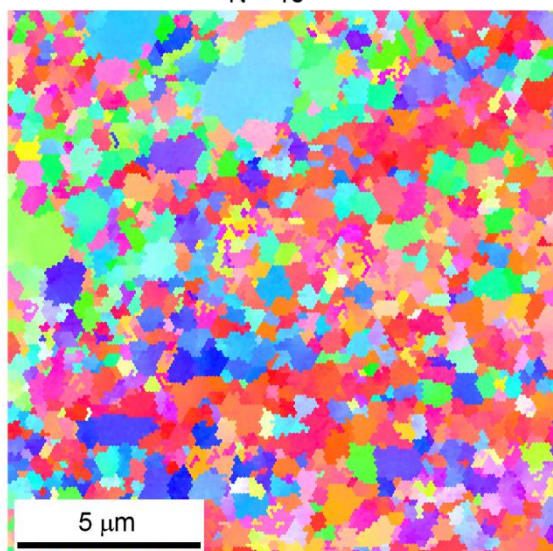


Figure 1 – Inverse pole figure maps of the microstructures at the mid-radius positions of samples processed by 1/8, 1/2 and 10 turns of HPT.

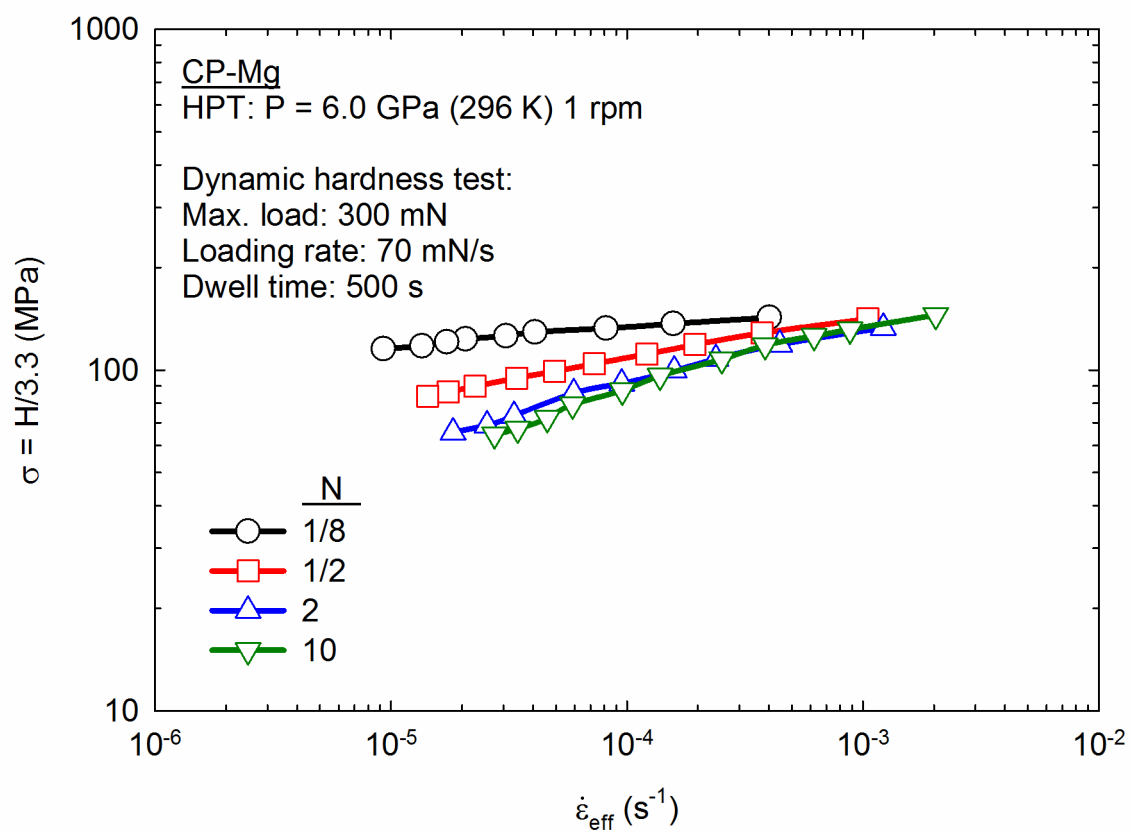


Figure 2 – Flow stress plotted as a function of the effective strain rate in dynamic hardness tests.

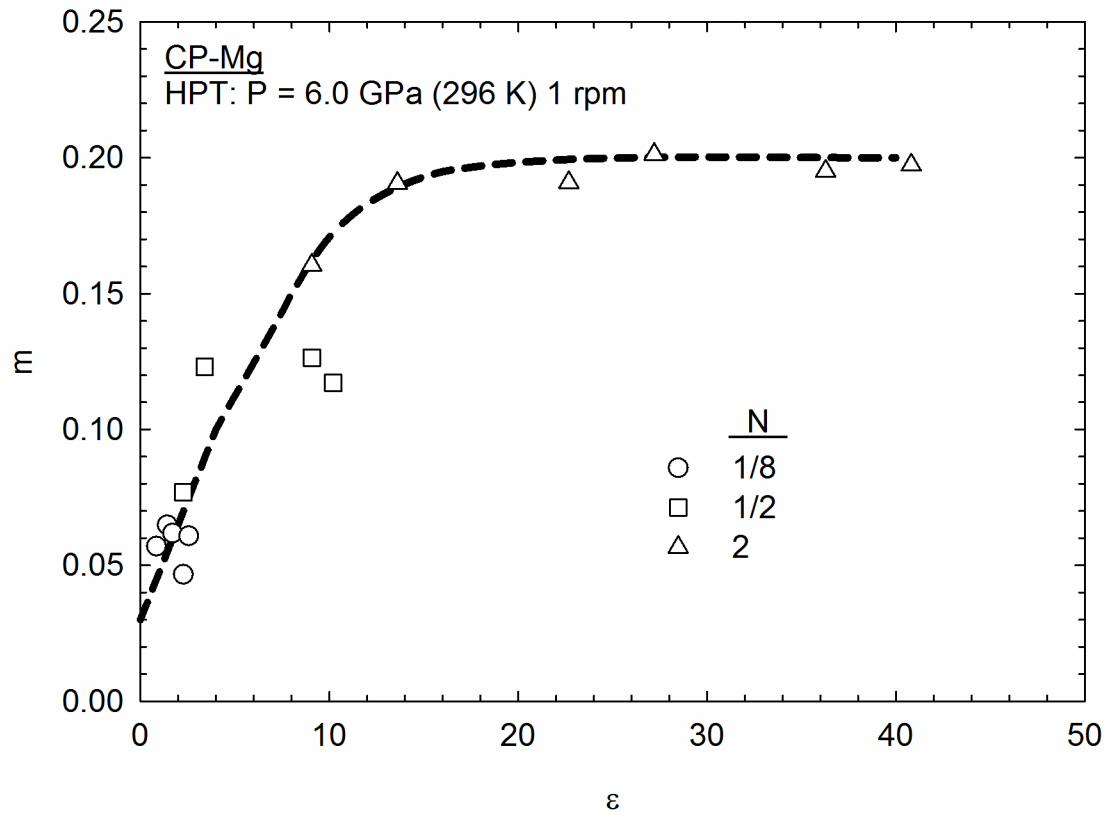


Figure 3 – Evolution of the strain rate sensitivity, m , as a function of the accumulated strain during HPT.

CP-Mg

HPT: 6.0 GPa (296 K) N = 10

Tensile test: T = 296 K

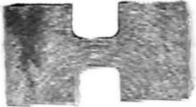





<u>Strain rate (s^{-1})</u>		<u>Elongation (%)</u>
Untested		
10^{-1}		20
10^{-2}		70
10^{-3}		130
10^{-4}		310
10^{-5}		360
<u>5 mm</u>		

Figure 4 – Appearance of the tensile specimens of samples processed by 10 turns of HPT and pulled to failure at different strain rates.

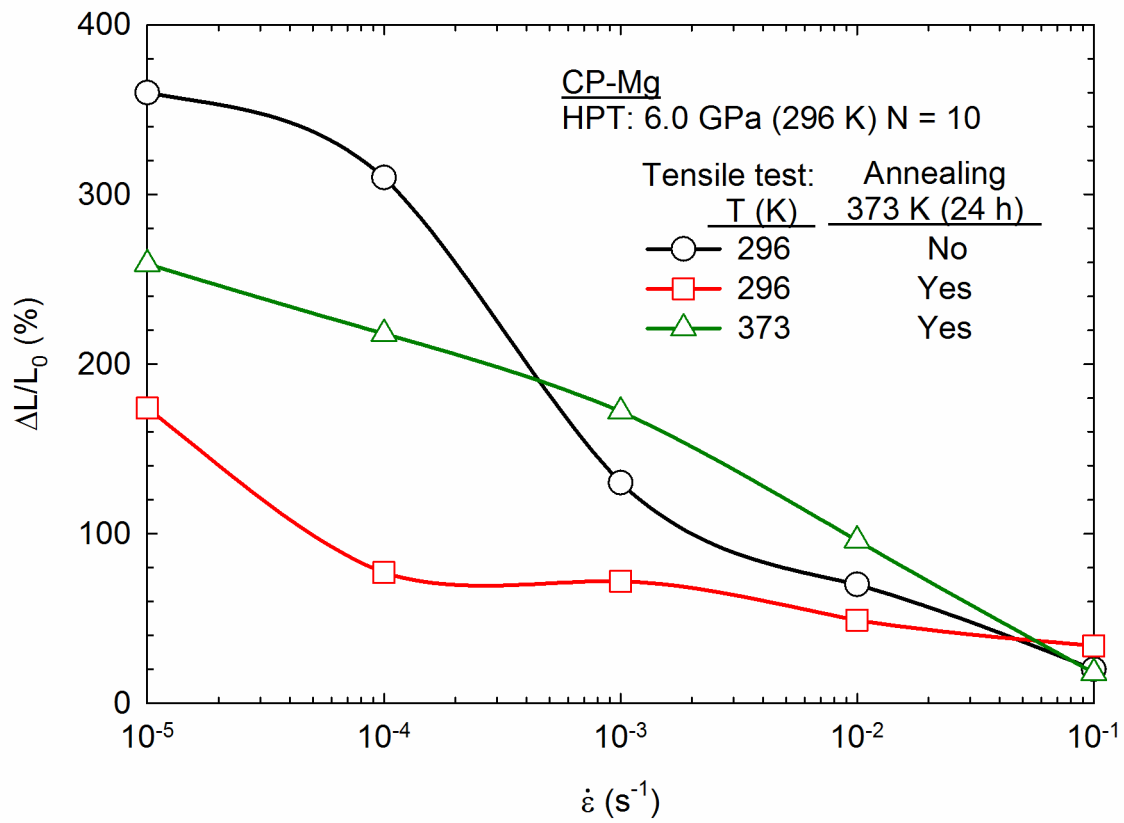


Figure 5 – Maximum elongations observed in samples of magnesium processed by HPT and tested in tension before and after annealing plotted as a function of the strain rate.

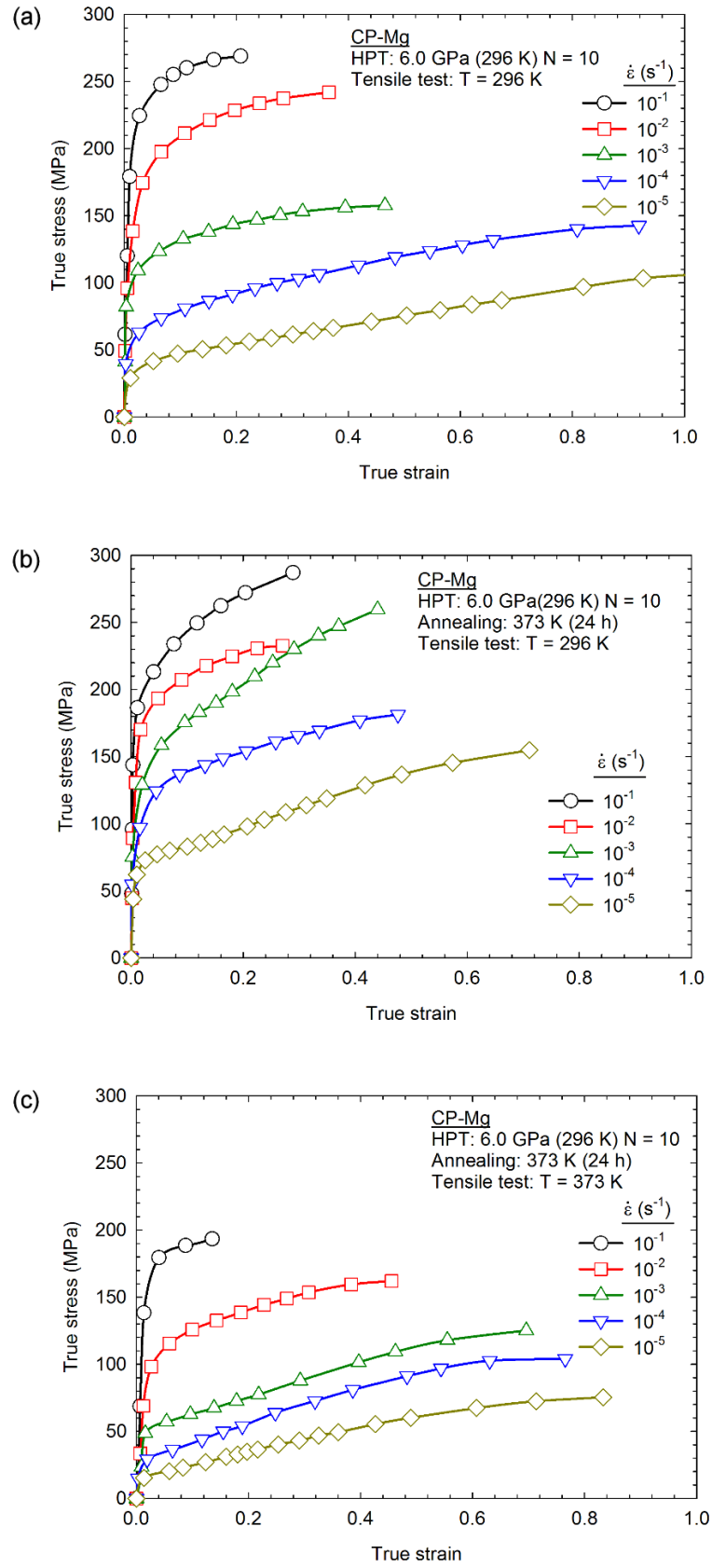


Figure 6 – True stress vs true strain curves for tensile testing of samples (a) processed by HPT and after annealing and testing at (b) room temperature and (c) 373 K.

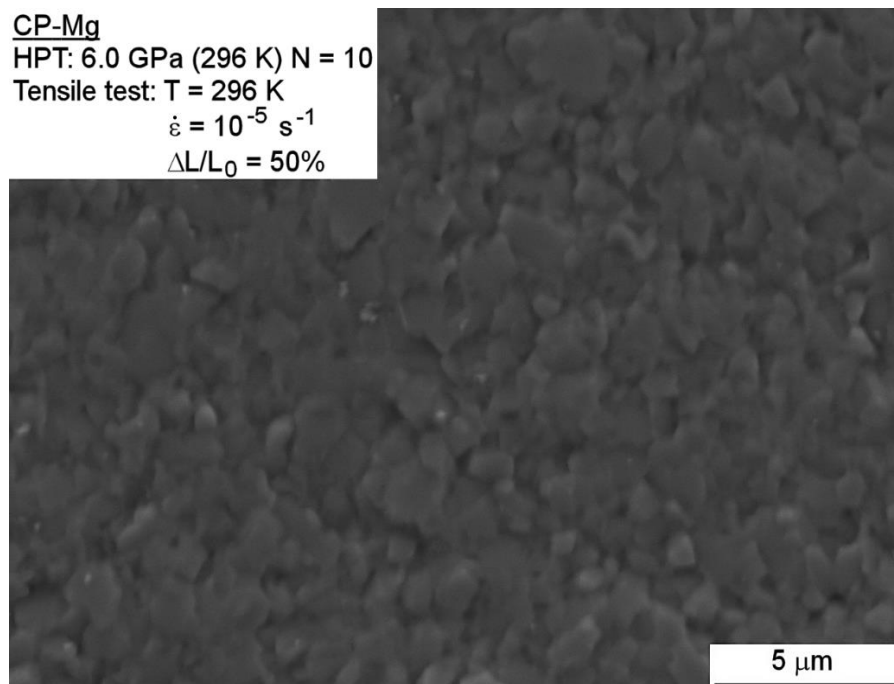


Figure 7 – Surface of tensile specimen processed by HPT and tested in tension at 10^{-5} s^{-1} to an elongation of 50%.

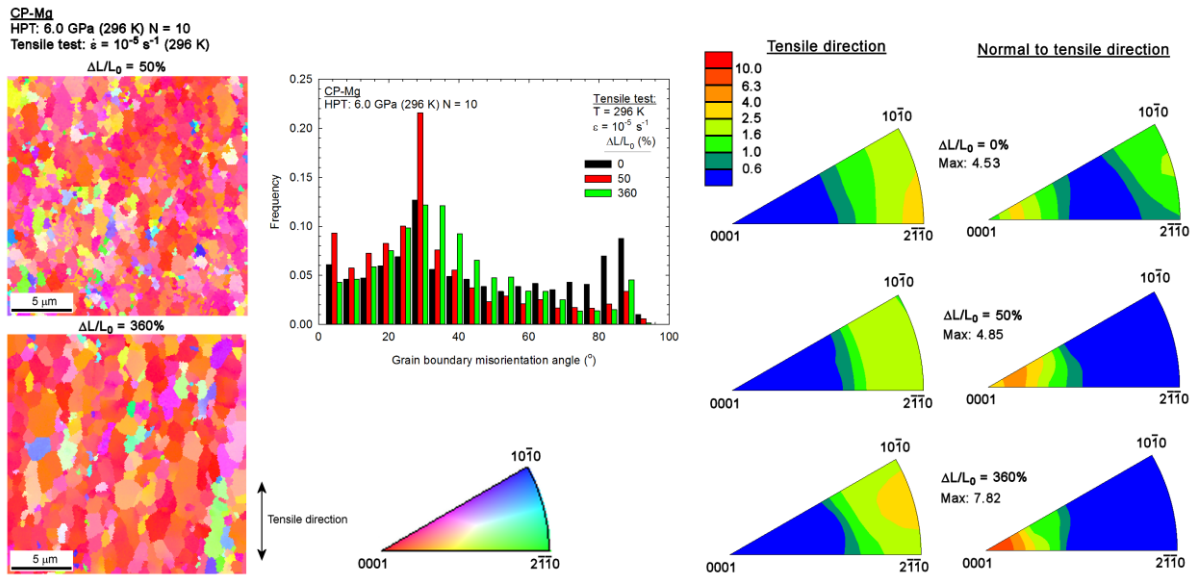
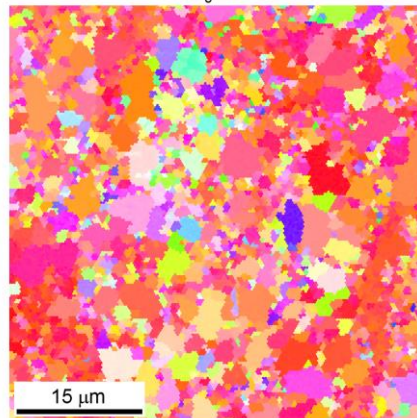


Figure 8 – Microstructures, grain boundary misorientation angle distributions and inverse pole figures in the gauge lengths of tensile specimens tested at room temperature at 10^{-5} s^{-1} to elongations of 50% and 360%.

CP-Mg
HPT: 6.0 GPa (296 K) 1 rpm, N = 10
Annealing: 373 K (24 h)
Tensile testing: T = 373 K, $\dot{\epsilon} = 10^{-5} \text{ s}^{-1}$
 $\Delta L/L_0 = 0\%$



$\Delta L/L_0 = 260\%$

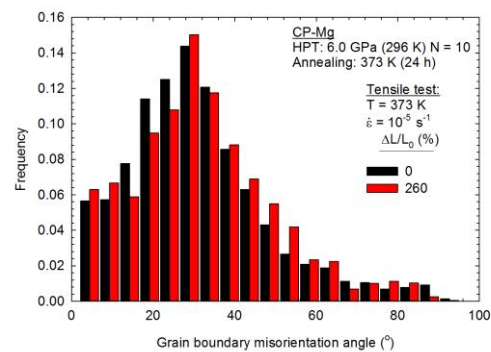
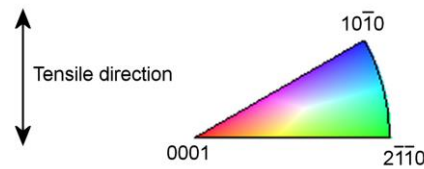
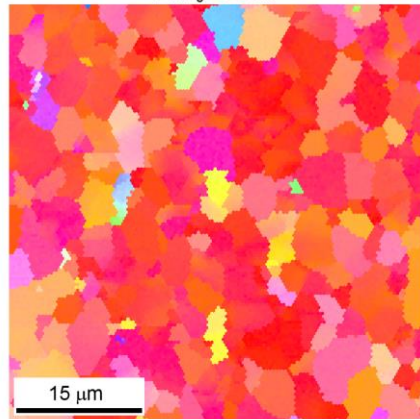


Figure 9 – Microstructures and grain boundary misorientation angle distributions in the gauge lengths before and after testing for tensile specimens processed by HPT and subjected to annealing.

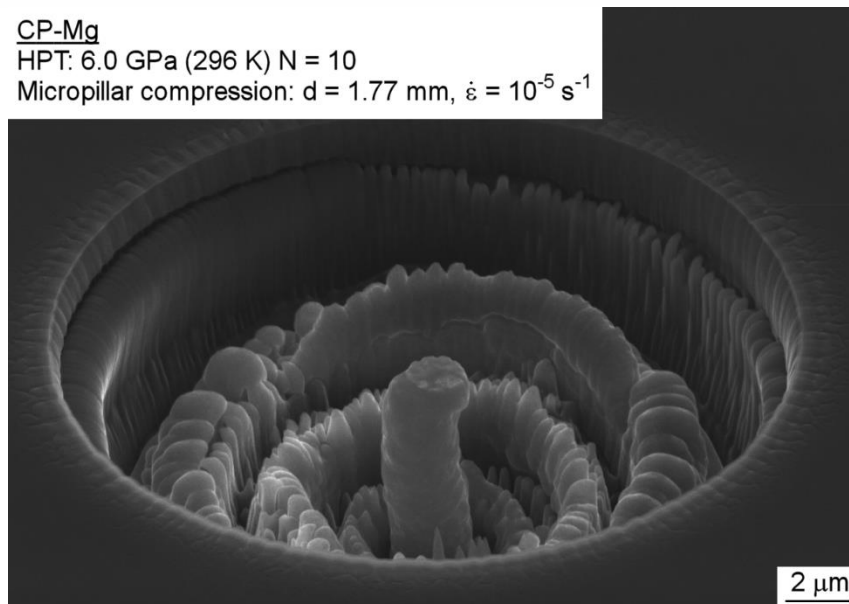
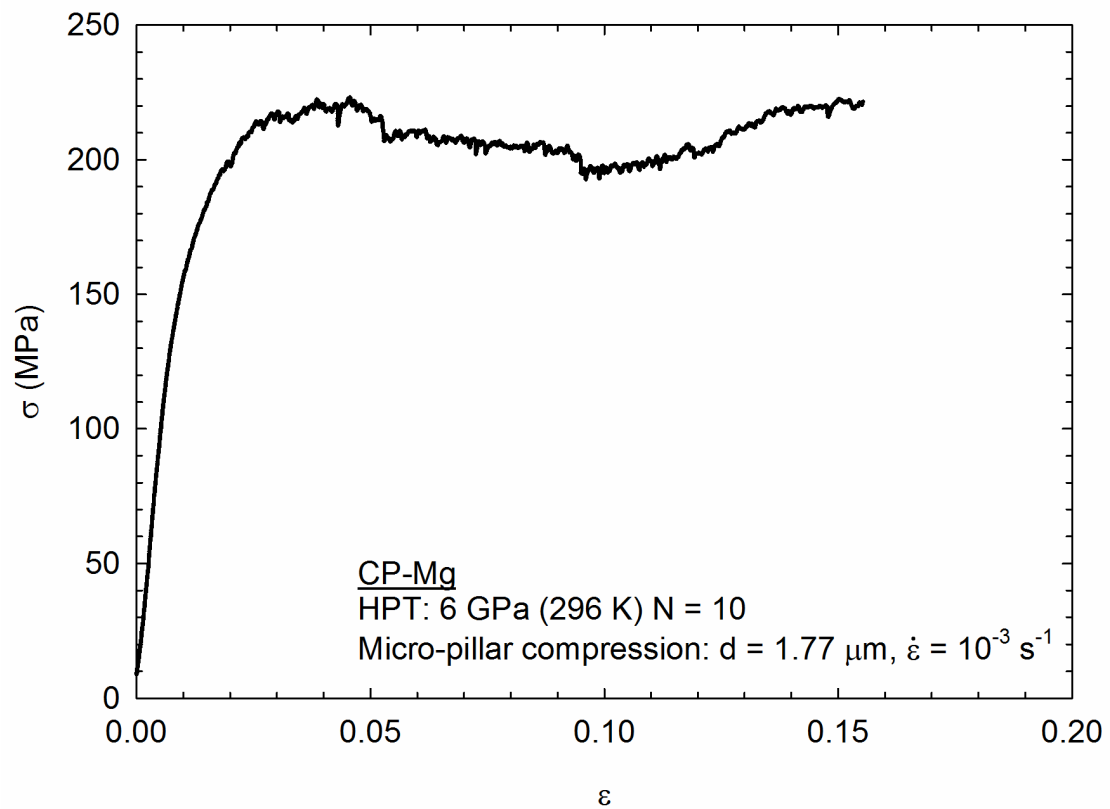


Figure 10 – Stress-strain curve determined by micropillar compression of a material processed by 10 turns of HPT (upper) and the appearance of the micropillar after ~15% strain (lower).

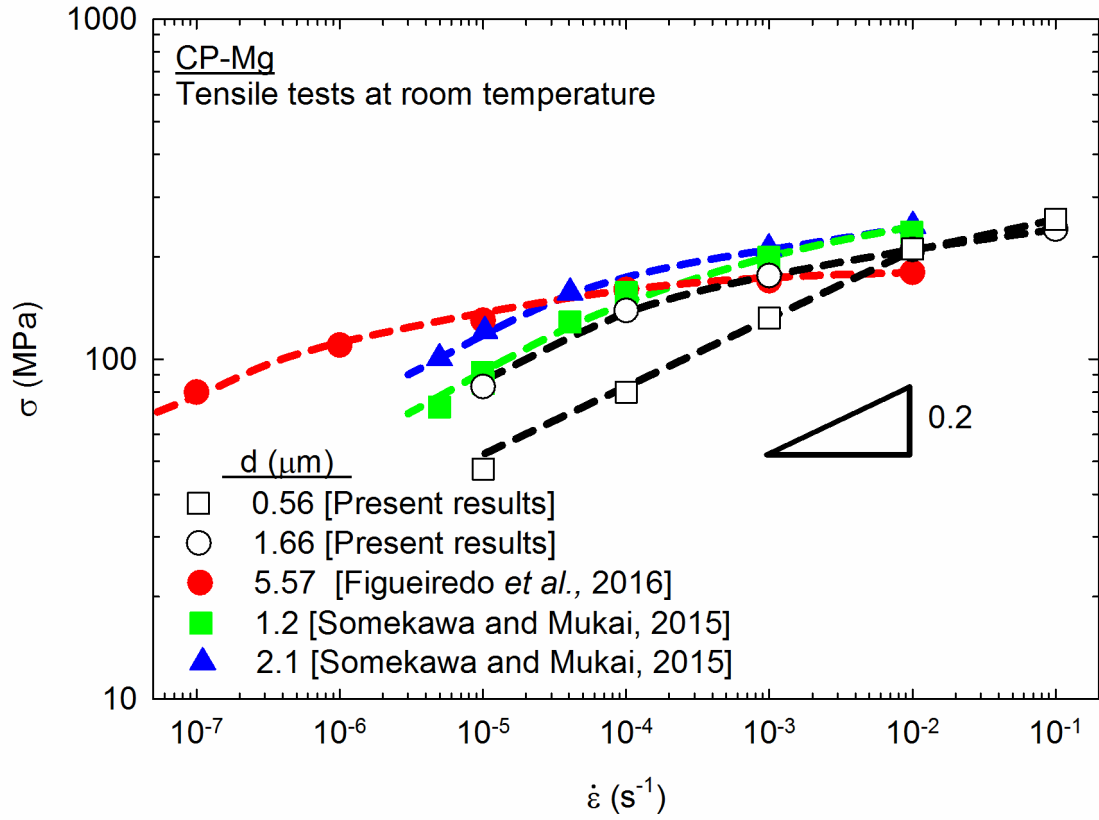


Figure 11 – Flow stress observed in tensile testing of fine-grained pure magnesium plotted as a function of the strain rate using the present results and published data [5,7].

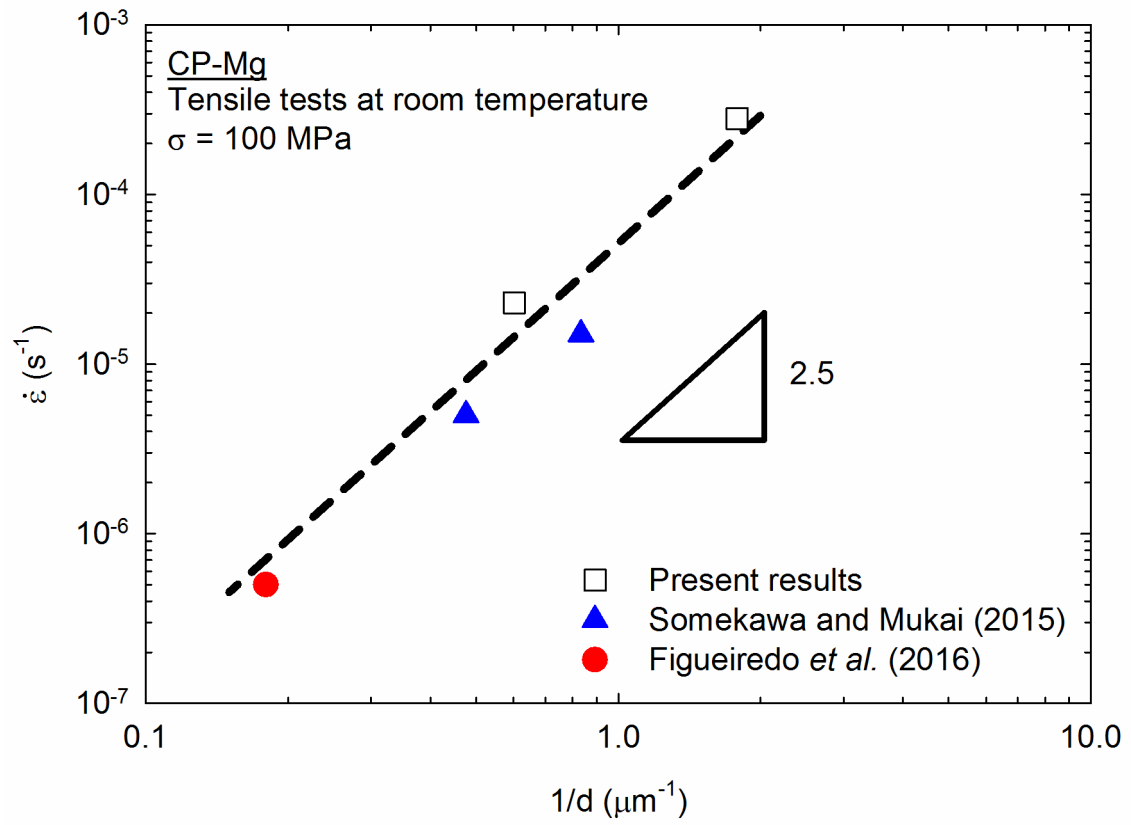


Figure 12 – Strain rate at a stress of 100 MPa plotted as a function of the inverse of the grain size using the present results and published data [5,7].

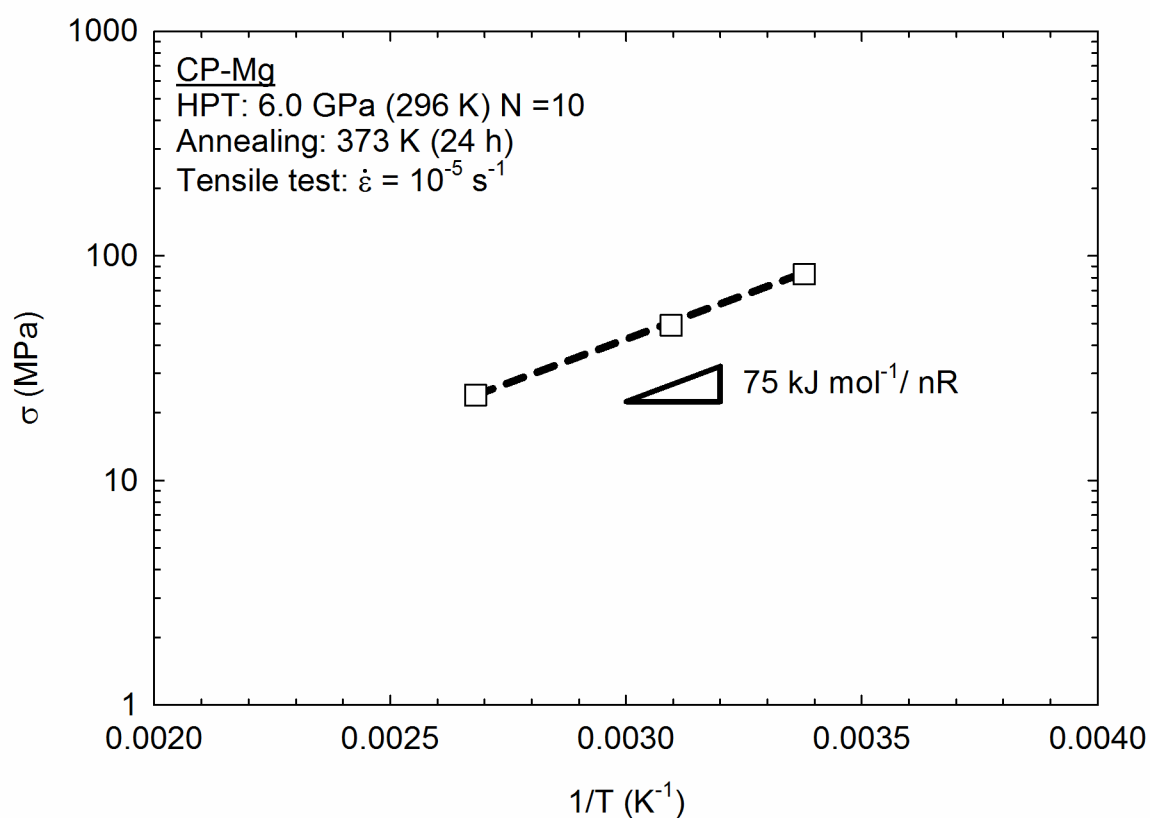


Figure 13 – Flow stress in the material annealed after HPT processing for tests at a strain rate of 10^{-5} s^{-1} plotted as a function of the inverse of the testing temperature.

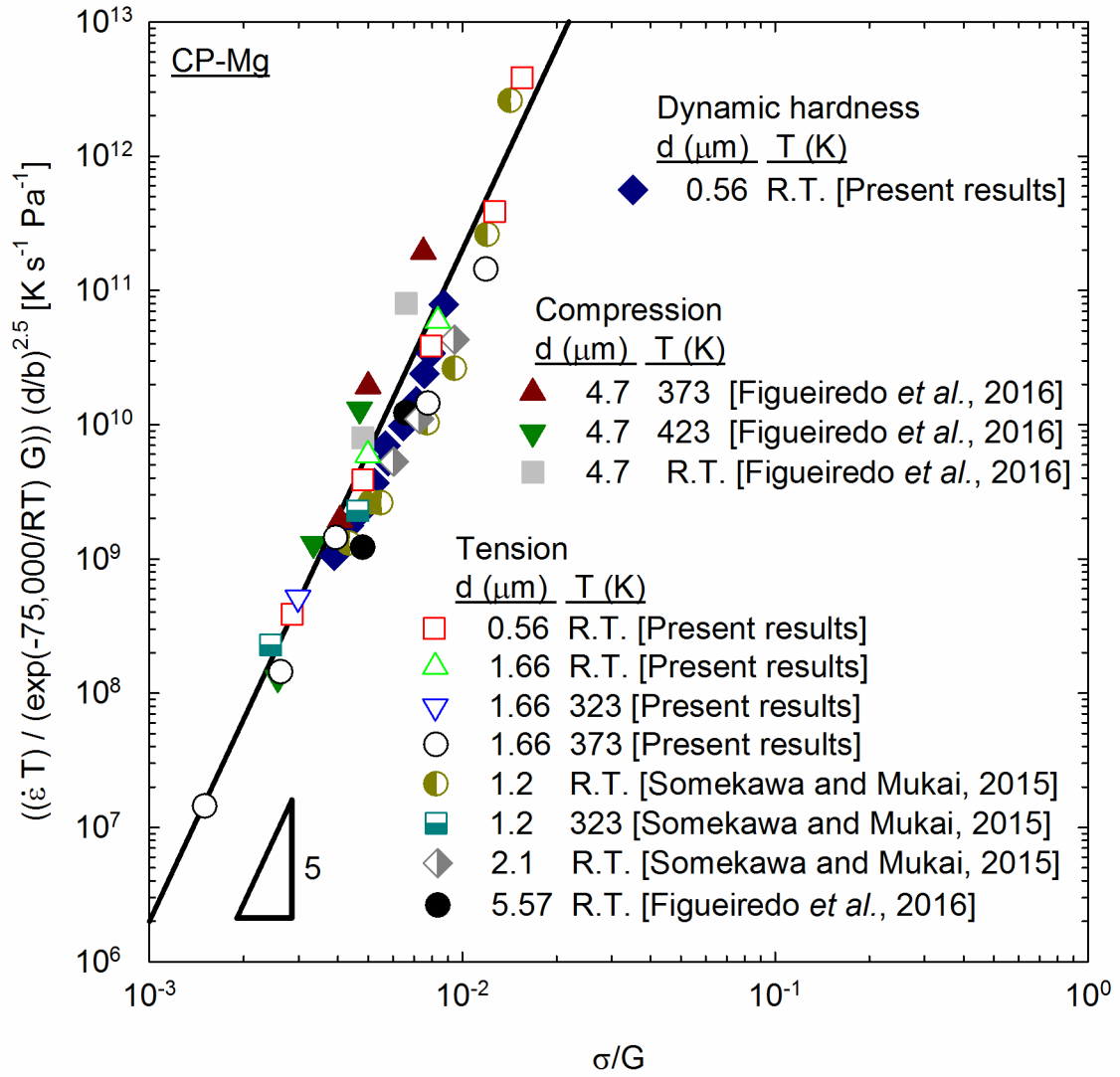


Figure 14 – Strain rate normalized by temperature and grain size plotted as a function of the flow stress normalized by the shear modulus for pure magnesium using the present results and reported data [5,7].